Observation of Resistive and Ferritic Wall Modes in a Line-Tied Pinch

W. F. Bergerson, D. A. Hannum, C. C. Hegna, R. D. Kendrick, J. S. Sarff, and C. B. Forest*

Department of Physics, University of Wisconsin-Madison, 1150 University Avenue, Madison, Wisconsin 53706

(Received 8 June 2008; published 4 December 2008)

The resistive wall mode is experimentally identified and characterized in a line-tied, cylindrical screw pinch when the edge safety factor is less than a critical value. Different wall materials have been used to change the wall time and show that the growth rates for the RWM scale with wall time and safety factor as expected by theory. The addition of a ferritic wall material outside the conducting shell leads to growth rates larger than the observed RWM and larger than theoretical predictions for the ferritic wall mode.

DOI: 10.1103/PhysRevLett.101.235005 PACS numbers: 52.58.Lq, 47.65.−d, 52.55.−s

A crucial issue for the attractiveness of many toroidal confinement concepts is the ability to stabilize long wavelength external kink modes which impose operational boundaries. While perfectly conducting walls can provide robust stabilization, a finite resistivity in the wall allows the stabilizing eddy currents in the wall to decay in time. On the time scale of a thin wall $\tau_w = \mu_0 \sigma_w r_w \delta_w$ (σ_w is the conductivity, r_w is the wall radius, and δ_w is the wall thickness with $\delta_w \ll r_w$) flux can leak through the wall and access the free energy available to the external kink. This mode, the resistive wall mode (RWM), then grows with a characteristic time τ_w.

Tokamak experiments are addressing RWM stabilization by controlling plasma rotation and by applying active feedback on magnetic coils [1–6], as are reversed field pinch experiments, where feedback stabilization has been used to simultaneously stabilize a spectrum of RWMs, allowing long pulse RFP operation with thin shells [7,8].

For fusion reactors, two advanced wall designs are under consideration which may directly impact the stability of the RWM. First, ferritic materials may be utilized because of their low activation to neutron radiation and ability to trim the magnetic field between coils (to reduce field errors). Second, flowing liquid lithium walls are being considered in part for heat removal and particle control. The presence of a ferritic boundary modifies the resistive wall mode into the ferritic wall mode (FWM), causing it to be more unstable [9,10]. Kurita reports that the β-limit is reduced to 90% of that without the ferromagnetic effect for a high aspect ratio tokamak. The magnetic quality of the wall pulls flux in and destabilizes the FWM while the RWM is still stable. The effect of a current driven external kink upon a line-tied mode structure is analogous to the effect of a pressure driven kink in a tokamak. Flowing liquid metal walls have the potential to passively stabilize the RWM [11–13].

In this Letter, several observations are reported from the Wisconsin rotating wall machine investigating the role of different electromagnetic boundary conditions on a current driven external kink mode in a linear pinch device (the cylindrical geometry is more amenable to future experiments using rotating walls). The first result is that the RWM has been clearly identified: line-tied external kink modes are observed (which have a different character than the internal kink modes previously reported in [14]) when the edge safety factor q_a is less than a critical value; different walls (with $\tau_w = 0.5$ ms and 7 ms) are used to show that the growth rates for the RWM scale with wall time and q_a and that the mode pitch changes with q_a as expected by theory. The second result is that the growth rate of the ferritic wall mode (studied by adding a Mumetal^{TM}shell outside the 7 ms shell) is significantly larger than expected by theory.

The theory of the external kink with line-tied ends has been developed for the idealized long-thin cylindrical geometry of a plasma of infinite conductivity with uniform current density, surrounded by perfect vacuum and resistive conducting walls [15–17]. In a periodic cylinder, the radial displacement of the perturbed magnetic field has the form $\tilde{\xi}_r(\theta, z) \sim e^{im\theta + in(2\pi/L)z}$, where m and n are mode numbers in the poloidal and axial directions. In the line-tied geometry the eigenmodes differ and take the form of standing waves

$$\tilde{\xi}_r(r, \theta, z) = f(r) e^{i\theta + i(2\pi/L q_a)((q_a/2)-1)z} \sin\left(\frac{n\pi z}{L}\right), \quad (1)$$

where $n = 1$, L is the distance between the two conducting end plates assumed to be line-tied, and q_a is given below. The boundary conditions of $\tilde{\xi}_r(0) = \tilde{\xi}_r(L) = 0$ are set by highly conducting copper plates at each end of the experiment.

The expression for the safety factor in the line-tied pinch is

$$q(r) = \frac{4\pi^2 r^2 B_z}{\mu_0 I_p(r) L}, \quad (2)$$

where r is the radius, B_z is the longitudinal magnetic field, and $I_p(r)$ is the amount of plasma current within radius r. $q(r)$ measures the helical twist in the field lines which varies with radius. $q_a \equiv q(a)$ is the safety factor at the plasma boundary.

Without a conducting wall, the line-tied external kink instability is given by the Kruskal-Shafranov condition: it is unstable when $q_a < 1$ [17–19] and grows on an Alfvén time scale. This differs from a periodic cylinder where the external kink is unstable near rational values of q_a. With a resistive wall the external kink has the same onset criteria; but a much slower growth rate. Theoretical understanding of the related FWM has been developed in the context of a long cylinder in [9]. With a single ferritic wall, the magnetic and resistive effects can be analytically decoupled. The resistive portion of the wall produces eddy currents in the wall capable of slowing external kink growth, while the magnetic nature of the wall is destabilizing. The magnetic wall amplifies the B_r signal from the external kink and mimics a positive feedback loop resulting in FWM instability.

The general formula for the RWM with ferromagnetic effects is

$$\gamma = \frac{2}{\tau_w}\left[\left(\frac{1-q_a}{q_a - 1 + (\frac{a}{b})^2}\right) + \left(\frac{\delta_w}{2_b}\right) \times \frac{(1-q_a)(\hat{\mu} + \hat{\mu}^{-1} - 2) + (\hat{\mu} - \hat{\mu}^{-1})(a/b)^2}{(a/b)^2 - 1 + q_a}\right], \quad (3)$$

where a is the plasma radius and $\hat{\mu}$ is the relative permeability of the magnetic material. This expression assumes a plasma with uniform current density and vacuum between the plasma (at a) and a single thin resistive and magnetic wall (at b). In deriving Eq. (3) corrections of order $(\frac{a}{L})$ are neglected in accordance with the long-thin approximation. The non ferritic wall case (RWM only) is obtained by setting $\hat{\mu} = 1$. While Eq. (3) is valid in the limit of a single wall, corrections must be considered for a geometry with either two resistive walls or one resistive and one magnetic wall. The correction for two distinct resistive walls (and wall times) at different radii is found in [17]. The growth rate for a two wall system (one magnetic and one resistive) can be solved for by matching the shape of the eigenmode solutions governed by the marginal ideal MHD equations in the plasma region to that governed by the sequence of vacuum and resistive/ferritic walls outside of the plasma. This approach is similar to Refs. [9,17].

The Wisconsin rotating wall machine (shown in Fig. 1) is 1.2 m long linear plasma device and has a plasma radius which can be varied from 3 to 10 cm. The plasma is produced by nineteen electrostatic plasma guns [20] packed in a hexagonal array, seen on the right side in the Fig. 1. Biasing the plasma guns with respect to the anode at the opposite end of the chamber generates an adjustable current (up to 1 kA/gun). The axial magnetic field from the electromagnets is nearly uniform but can be adjusted to have a mild mirror ratio. For results here $|B_z| =$ 250—400 G with $0.95 < R_m < 1.2$, where $R_m \equiv B_{L=0m}/B_{L=0.6m}$. The plasma has an electron density of $\approx 4 \times 10^{13}$ cm^{-3} and an electron temperature of ≈ 5 eV. The size of the plasma and current profile from a single gun

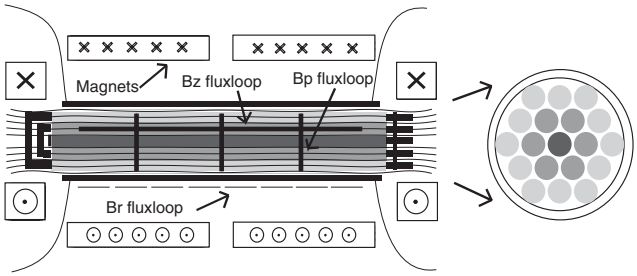

FIG. 1. A schematic of the line-tied pinch experiment. The solenoidal magnets produce either a nearly uniform magnetic field or a magnetic bottle between the two ends. The anode plate is on the left and drawn to highlight its the electrical connectivity. The hexagonally packed cathode array of plasma guns (shown on the right), breaks into three independently controllable regions of plasma represented by shadings in gray. The B_r flux loops lay against the outside wall of the vessel, while the B_z and B_p coils are just inside the wall.

has been measured to have a gaussian profile with a half maximum radius of approximately 2 cm; the gun-to-gun spacing is 3.5 cm thus providing a current source which varies by less than 25%. There is also expected to be an additional merging of the current filaments, such as that observed in Refs. [21] and simulated in [22] to smooth out the azimuthal variation of the current profile. Plasmas formed by the central seven guns are about 6 cm in radius. A conducting plate surrounding the gun nozzles and the conducting anode at opposite end of the plasma are expected to create line-tying boundary conditions for pulse lengths less than 200 ms. Unlike other linear devices [23,24] which report kinks in the context of one free and one line-tied end, the threshold of external kink stability reported herein is consistent with two line-tied ends.

Three different wall configurations are studied in the experiment. The first is the 10 cm inner radius stainless steel vacuum vessel that has $\tau_w = 0.5$ ms. The second is a two wall system consisting of the vacuum vessel surrounded by a copper shell that has a composite $\tau_w =$ 7 ms. Finally, to explore the FWM, a 0.2 mm thick Mumetal^{TM} foil has been wrapped on top of the copper shell. For this final scenario, the inner shells ($\tau_w = 7$ ms) are surrounded by a resistive magnetic wall ($\tau_w \approx 60$ μs). The magnitude of the growth rate is determined principally by the longest wall time in the system using permeability of vacuum (here, this would be the 7 ms wall), but the critical q_a is increased and determined by the relative permeability of the magnetic material $\hat{\mu}$. As $\hat{\mu} \rightarrow 1$, mode onset occurs when $q_a = 1$. For the Mumetal^{TM} used in this experiment and an applied field of $B_z \sim$ 300 G, $\hat{\mu} \approx 1200$. The theoretical growth rates are summarized in Fig. 2. The solid black trace is generated with Eq. (3) by setting $\hat{\mu} = 1$ and $\tau_w = 0.5$ ms. The correction for two resistive walls is given in [17] and plotted in solid red. Finally, the FWM mode growth for two walls (one

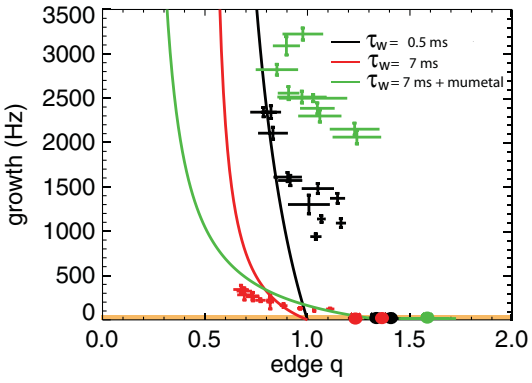

FIG. 2 (color). Measured and predicted growth rates for the FWM and RWM in a line-tied pinch. The black and red lines correspond to the theoretical predictions for the RWM with purely resistive walls with $\tau_w = 0.5$ ms and 7 ms, respectively, while the green line corresponds to the FWM. Experimentally measured values for the three cases are overplotted. The standard deviation of measured growth rates is used in determining the error in the growth rate. The horizontal error bars reflect the error in a in the measurement of q_a. The orange bar is the minimum resolvable growth rate. Stable plasmas are marked by solid circles.

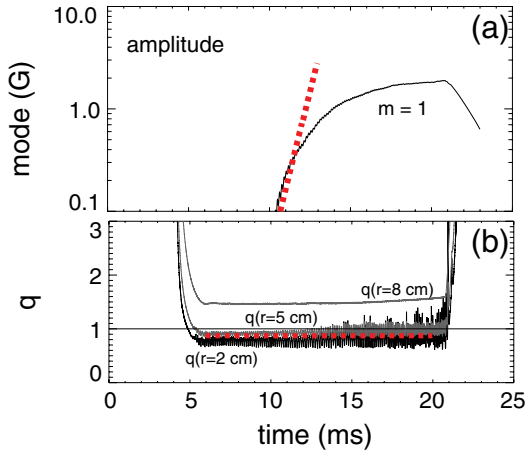

FIG. 3 (color online). Typical resistive wall mode. In (a) the amplitude of the $m = 1$ mode as determined by a spectral analysis of the spatial variation in $B_r(\theta)$ at a fixed Z location (near the anode). The dashed red trace is the exponential fit to the data from 10 to 14 ms. For reference (b) shows the evolution of the q profile as monitored by the segmented anode. The estimate for q_a is given by the red dashed line.

magnetic and one resistive) is plotted in solid green. The two resistive walls in the experiment are modeled as a single resistive wall because their effective wall time is dominated by the copper wall.

The q profile is estimated by measuring the current flowing to each of three concentric rings which make up the anode endplate (outer radii of 0.023, 0.052, and 0.081 m, respectively). The flux surfaces associated with the magnetic field from the magnets are numerically calculated, and then the field line equations are numerically integrated to evaluate the field line twist. The enclosed axial current is assumed to be a function of flux.

The MHD activity is monitored by an array of 120 flux loops and Mirnov coils inside and outside the shell. B_p and B_z are measured by Mirnov coils inside the stainless vessel: ten coils measuring B_z are distributed along the machine axis, three arrays of B_θ coils (ten coils spaced evenly in θ) are located at three locations along the machine axis. Eighty flux loops monitor B_r outside the shell. The flux loops consist of 6.5 cm $\times$ 12.5 cm coils that provide a full two-dimensional structure of $B_r(r = a, \theta, z, t)$ at the plasma boundary. The signals from the flux loops and Rogowski coils used for monitoring currents undergo analog integration prior to digitization.

An example of a typical discharge with the RWM instability is shown in Fig. 3 for the $\tau_w = 7$ ms case. The RWM grows in time with a clear $m = 1$ kink mode signature, as seen in the two-dimensional surface measurement of B_r in Fig. 4. The dependence of the mode's pitch on q_a [as predicted by Eq. (1)] and amplitude can be seen by comparing Figs. 4(a) and 4(b). The lower the value for q_a, the tighter the twist and larger the mode amplitude. In Fig. 4, the heavy black line highlights the degree of twist in the mode.

The measured RWM growth rates are displayed in Fig. 2 for comparison to the theoretical values. The black and red points are from plasmas with $\tau_w = 0.5$ ms and $\tau_w = 7$ ms, respectively. The green points are the FWM growth rates with $\tau_w \approx 7$ ms and $\hat{\mu} = 1200$. The data are color coded to the corresponding theoretical growth rates (solid lines). RWM onset for $\tau_w = 0.5, 7$ ms occurs between $1.1 < q_a < 1.3$. The safety factor is adjusted by increasing the plasma current while holding B_z constant on a shot to shot basis,

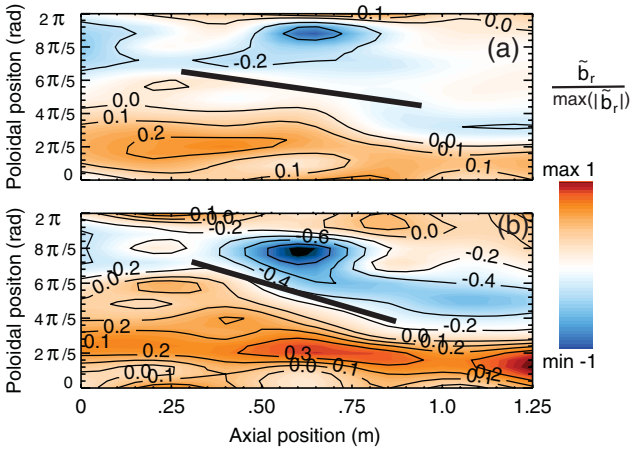

FIG. 4 (color). Normalized contour plots of B_r for the RWM. In (a) the RWM when $q_a \approx 0.8$. In (b) the RWM when $q_a \approx 0.6$. Note the $m = 1$ character in both plasmas as well as the dependence of the axial structure on q_a. A lower q_a translates into a tighter twist in the eigenmode of the RWM.

from Eq. (2) it can be seen that this process varies q_a. Mode growth itself is calculated by fitting an exponential to the mode amplitude during its initial growth phase as seen in Fig. 3(a).

Qualitatively, the RWM agreement is good: the wall time sets the growth rate, and the plasma becomes more unstable as q is driven lower. When $\tau_w = 0.5$ ms, the mode grows in the kHz range; conversely, the mode grows an order of magnitude slower when $\tau_w = 7$ ms. The growth rate of the RWM in B_p (not shown) has been measured and found to match that of B_r. FWM onset is in good agreement with predictions at $q_a \cong 1.4$; the mode becomes unstable at a higher q_a than observed with the resistive walls alone. Remarkably, however, the FWM growth rates are approximately an order of magnitude larger than the $\tau_w = 7$ ms wall.

The imperfect agreement between theoretical and experimental RWM measurements may come from a variety of sources. First, the theory used to derive mode stability assumes an ideal plasma with a uniform current and plasma density inside a, perfect cylindrical symmetry, and a vacuum region for $a < r < b$. In the machine, the experimental current and density profiles have a radial dependence (that also vary gradually in the axial direction as a result of finite cross-field diffusion). The current carrying plasma is also surrounded by a low density plasma in the region $a < r < b$ which complicates the determination of a. Second, the estimation of q is based upon measurement of the current profile at the anode end, and takes no account of variations of current density along the plasma column. Future measurements of the current profile will attempt to quantify the axial variation. Third, the effects of plasma flow and resistivity are not considered by the theoretical model of the external kink. The guns provide an ion flow at a fraction of the ion sound speed and, as described in [25], may lead to growth when $q_a > 1$. The plasma has a finite temperature (5–10 eV) and resistive effects may modify the stability of the external kink as expected for internal kink modes [26,27].

The large difference between measured and expected growth rates for the FWM is not easily explained. The impact of the Mumetal™ on the plasma configuration appears minor. The vacuum axial magnetic field was measured to be altered less than 5% at the field strengths used in these experiments. Despite plasmas being produced in the same manner, the current profile observed with the ferromagnetic wall was somewhat broader than for the copper and stainless steel wall. However, this modification to the current profile is expected to be less important than the factors of resistivity, plasma flow, and asymmetry in the plasma discussed in relation to the RWM. The disagreement between the predicted and measured FWM growth rates therefore suggests the model used to predict the mode may not be complete.

In summary, clear evidence for the resistive wall mode in a linear line-tied plasma has been obtained. Growth rates agree with theory in magnitude and scaling with q_a. The growth of the observed FWM is much faster than expected; however, mode onset occurs at a higher q_a than observed with resistive walls and is in agreement with predictions. While detailed comparisons with theories that account for finite plasma resistivity and flow remain to be performed, it is unlikely that these corrections can account for the discrepancy with the FWM observations.

This work was supported by the U.S. DOE.

*cbforest@wisc.edu

[1] T. Ivers *et al.*, Phys. Plasmas **3**, 1926 (1996).
[2] C. Bishop, Plasma Phys. Controlled Fusion **31**, 1179 (1989).
[3] A. Garofalo *et al.* (DIII-D team), Phys. Plasmas **6**, 1893 (1999).
[4] E. Strait *et al.* (DIII-D team), Phys. Plasmas **11**, 2505 (2004).
[5] H. Reimerdes *et al.*, Phys. Rev. Lett. **98**, 055001 (2007).
[6] S. Sabbagh *et al.*, Phys. Rev. Lett. **97**, 045004 (2006).
[7] P. Brunsell *et al.*, Phys. Rev. Lett. **93**, 225001 (2004).
[8] R. Paccagnella *et al.*, Phys. Rev. Lett. **97**, 075001 (2006).
[9] G. Kurita *et al.*, Nucl. Fusion **43**, 949 (2003).
[10] K. Tsuzuki *et al.*, Nucl. Fusion **46**, 966 (2006).
[11] C. G. Gimblett, Nucl. Fusion **31**, 2183 (1990).
[12] J. P. Freidberg and R. Betti, Phys. Plasmas **8**, 383 (2001).
[13] M. V. Umansky, R. Betti, and J. P. freidberg, Phys. Plasmas **8**, 4427 (2001).
[14] W. F. Bergerson *et al.*, Phys. Rev. Lett. **96**, 015004 (2006).
[15] I. Lanskii and A. Shchetnikov, Sov. J. Plasma Phys. **16**, 322 (1990).
[16] D. D. Ryutov, R. H. Cohen, and L. D. Pearlstein, Phys. Plasmas **11**, 4740 (2004).
[17] C. Hegna, Phys. Plasmas **11**, 4230 (2004).
[18] V. Shafranov, At. Energy (N.Y.) **5**, 38 (1954).
[19] M. Kruskal and M. Schwarzschild, Proc. R. Soc. A **223**, 348 (1954).
[20] G. Fiksel, *et al.*, Plasma Sources Sci. Technol. **5**, 78 (1996).
[21] I. Furno *et al.*, Phys. Plasmas **12**, 055702 (2005).
[22] H. Takamaru and T. Sato, Phys. Plasmas **4**, 2845 (1997).
[23] I. Furno *et al.*, Phys. Rev. Lett. **97**, 015002 (2006).
[24] I. Furno *et al.*, Phys. Plasmas **14**, 022103 (2007).
[25] D. Ryutov, T. Intrator, S. Abbate, and T. Madziwa-Nussinov, Phys. Plasmas **13**, 032105 (2006).
[26] G. L. Delzanno, E. G. Evstatiev, and J. M. Finn, Phys. Plasmas **14**, 092901 (2007).
[27] G. L. Delzanno and J. M. Finn, Phys. Plasmas **15**, 032904 (2008).